Spin selectivity effect in achiral molecular systems

Ai-Min Guo,[1,*] Ting-Rui Pan,[2] Tie-Feng Fang,[3] X. C. Xie,[2,4] and Qing-Feng Sun[2,4,†]

[1]*Department of Physics, Harbin Institute of Technology, Harbin 150001, China*
[2]*International Center for Quantum Materials, School of Physics, Peking University, Beijing 100871, China*
[3]*Center for Interdisciplinary Studies and Key Laboratory for Magnetism and Magnetic Materials of MOE, Lanzhou University,*
Lanzhou 730000, China
[4]*Collaborative Innovation Center of Quantum Matter, Beijing 100871, China*

Recently, chiral-induced spin selectivity has been attracting intense interest. Here, we report a theoretical study of spin-dependent electron transport in achiral nanotubes contacted by nonmagnetic leads. Our results reveal that by properly connecting to the leads, the achiral nanotubes can present a pronounced spin filtering phenomenon even if the spin-orbit coupling is very weak. In addition, the spin selectivity effect holds for various achiral nanotubes with different radii and is still significant in the presence of strong disorder and dephasing. These findings open new opportunities of using achiral molecules in spintronic applications and could motivate further studies on spin transport along achiral systems.

I. INTRODUCTION

Spintronics aims at manipulation of the electron-spin injection, transport, and detection in solid-state systems, and at utilizing the electron spin to carry and process information. This multidisciplinary field has been receiving extensive and growing attention [1–5], owing to low power consumption of spintronic devices and fundamental scientific interest. As compared with conventional inorganic metals and semiconductors, organic molecules possess superior advantages of long spin lifetimes, chemical flexibility, low production costs, and compatibility with biological tissues, and are thus considered as an ideal candidate in spintronic applications [6–9]. The spin transport properties have been widely reported in molecular systems, including organic spin valves [10–14], single-molecule magnets [15–17], and molecular spin transistors [18–20]. All these spin effects originate from the components of either magnetic materials or heavy atoms with extremely large spin-orbit coupling (SOC).

Chiral molecules are those that have no plane of symmetry and cannot be superimposed on their mirror images, just like one's left and right hands. One of the most famous chiral molecules is double-stranded DNA. Recent works made an important breakthrough in the field of spintronics, finding a pronounced spin filtering phenomenon in the chiral molecules. It was reported in two experiments that the DNA molecules can serve as an efficient spin filter [21,22], i.e., they can discriminate between spin-up electrons and spin-down ones. These experimental observations are surprising, because the DNA molecules are nonmagnetic and the SOC strength is small. The corresponding effect is termed chiral-induced spin selectivity [23]. Since then, the chiral-induced spin selectivity has been attracting intense interest, and has been extensively demonstrated in the DNA molecules [21,22,24–28], α-helical proteins [29–32], DNA-wrapped carbon nanotube hybrids [33,34], helicenes [35], and other helical systems [36–41]. All

these studies focus on the chiral/helical molecules, unveiling that the helical symmetry is a prerequisite ingredient to yield spin-selective electron transmission.

Besides the chiral molecules, there exist many other molecules which do have a plane of symmetry and are superimposable upon their mirror images. This type of molecules is known as achiral molecules which lack the helical symmetry and are ubiquitous for synthetic materials (see Ref. [42] for a review and Refs. [43–49] for achiral nanotubes). Can the spin selectivity effect appear in the achiral molecules? In this paper, we give a definite answer to this issue, finding that the helical symmetry may not be necessary for the emergence of the spin selectivity effect. A model Hamiltonian is proposed to explore quantum spin transport along two-terminal achiral nanotubes, which are contacted by left and right nonmagnetic leads (Fig. 1). Here, we point out that each lead connects to a single site of the nanotubes, which can be realized through chemisorption mediated by thiol groups [22,50]. By properly connecting to the leads, the achiral nanotubes can present pronounced spin selectivity effect, even for very weak SOC strength. This spin filtering phenomenon arises from the breaking of mirror symmetry, which is caused by contact asymmetry between the left/right lead and the molecules, although the molecules themselves are achiral. Additionally, the spin selectivity effect is robust against perturbations, and remains significant in the presence of strong disorder and dephasing. These results expand the spin selectivity effect to a family of the achiral molecular systems and will facilitate designing molecule-based spintronic devices.

The rest of the paper is organized as follows. In Sec. II, we obtain a model Hamiltonian to describe spin-dependent electron transport along the achiral nanotubes. In Sec. III, the spin polarization and conductances are numerically calculated for the achiral nanotubes by considering a variety of contact situations. Finally, the results are summarized in Sec. IV.

II. MODEL

The spin transport along the two-terminal achiral nanotubes, as illustrated in Fig. 1, can be simulated by the

---

*amguo@hit.edu.cn
†sunqf@pku.edu.cn
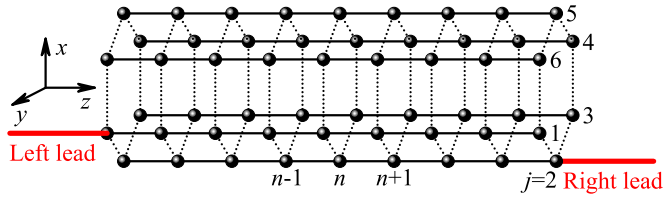
FIG. 1. Schematic view of an achiral nanotube (no helical symmetry) whose sites {1,1} and {2,N} are coupled to left and right one-dimensional nonmagnetic leads, respectively. The index {j,n} denotes site n of chain j. Here, the number of chains is $J = 6$.

Hamiltonian:

$$\mathcal{H} = \mathcal{H}_0 + \mathcal{H}_{el} + \mathcal{H}_d, \tag{1}$$

where the Hamiltonian $\mathcal{H}_0 = \mathcal{H}_{nt} + \mathcal{H}_{so}$, $\mathcal{H}_{nt} = \hat{\mathbf{p}}^2/2m + V$ describes the kinetic and potential energies of the electron, and $\mathcal{H}_{so} = (\hbar/4m^2c^2)\nabla V \cdot (\hat{\sigma} \times \hat{\mathbf{p}})$ is the SOC term. Here, $\hat{\mathbf{p}}$ is the momentum operator, m is the electron effective mass, $\hbar$ is the reduced Plank constant, c is the speed of light, and $\hat{\sigma} = (\sigma_x, \sigma_y, \sigma_z)$ with $\sigma_{x,y,z}$ being the Pauli matrices. Following the procedure of Ref. [30], $\mathcal{H}_0$ is expressed as

$$\mathcal{H}_0 = \sum_{j=1}^{J} \left[\sum_{n=1}^{N} \varepsilon_{jn} c_{jn}^\dagger c_{jn} + \sum_{n=1}^{N-1} c_{jn}^\dagger (t_\parallel + 2is\sigma_j) c_{j,n+1} \right.$$
$$\left. + \sum_{n=1}^{N} c_{jn}^\dagger (t_\perp + 2i\mu\sigma_z) c_{j+1,n} + \text{H.c.} \right]. \tag{2}$$

Here, $c_{J+1,n}^\dagger \equiv c_{1n}^\dagger$ and $c_{jn}^\dagger = (c_{jn\uparrow}^\dagger, c_{jn\downarrow}^\dagger)$ is the creation operator at site {j,n} of the nanotube, with the index {j,n} standing for site n of chain j. J is the number of chains and N is the nanotube length; ε_{jn} is the potential energy, $t_\parallel$ ($t_\perp$) is the intrachain (interchain) hopping integral, and s [$\mu = s\cos(\Delta\phi/2)$] is the intrachain (interchain) SOC parameter; $\sigma_j = \sigma_x \sin\phi_j - \sigma_y \cos\phi_j$, with $\Delta\phi = 2\pi/J$ and $\phi_j = (j-1)\Delta\phi$ the azimuth of site {j,n} in the cylindrical coordinate system. We point out that when $J = 2$, Eq. (2) is reduced to the previous model without the helical symmetry [24]. Consequently, one may expect that no spin filtering phenomenon could be observed in the electron transmission along the achiral molecules.

The Hamiltonian $\mathcal{H}_{el} = \sum_k [\varepsilon_k(a_{Lk}^\dagger a_{Lk} + a_{Rk}^\dagger a_{Rk}) + \tau(a_{Lk}^\dagger c_{11} + a_{Rk}^\dagger c_{jN} + \text{H.c.})]$ describes the left and right nonmagnetic leads and their couplings to the molecule. We emphasize that the left lead is always coupled to site {1,1} of the molecule and the right lead is attached by site {j,N}, e.g., $j = 2$ in Fig. 1. Finally, the Hamiltonian $\mathcal{H}_d = \sum_{j,n,k}(\varepsilon_{jnk} d_{jnk}^\dagger d_{jnk} + t_d d_{jnk}^\dagger c_{jn} + \text{H.c.})$ depicts dephasing processes in the experiments, with $d_{jnk}^\dagger = (d_{jnk\uparrow}^\dagger, d_{jnk\downarrow}^\dagger)$ the creation operator of mode k in Büttiker's virtual leads [24,51]. During the charge transport process, an electron may suffer inelastic scatterings from, e.g., phonons, nuclear spins, and impurities, which lead to the loss of phase memory of the electron. These dephasing processes can be described by connecting each site of the molecule to one Büttiker virtual lead. The spin-up conductance $G_\uparrow$ and spin-down one $G_\downarrow$ of this system can be obtained from the

Landauer-Büttiker formula and the nonequilibrium Green's function [52], by imposing the boundary condition that the net current across every virtual lead is zero. The spin polarization is then calculated by $P_s = (G_\uparrow - G_\downarrow)/(G_\uparrow + G_\downarrow)$.

In the numerical results presented below, the hopping integrals $t_\parallel = t_\perp = t$ and the coupling $\Gamma_{L/R}$ to the left/right lead are taken as the energy unit, $t = \Gamma_{L/R} = 1$. The nanotube potential energy, the SOC strength, and the couplings to Büttiker's virtual leads are chosen to be $\varepsilon_{jn} = 0$, $s = 0.05$, and $\Gamma_d = 0.04$, respectively, unless stated otherwise. Notice that the system has electron-hole-type symmetry when J is even, viz., the Hamiltonian in Eq. (1) is invariant under the transformation $c_{jn\uparrow} \to (-1)^{j+n} c_{jn\downarrow}^\dagger$ and $c_{jn\downarrow} \to (-1)^{j+n+1} c_{jn\uparrow}^\dagger$. Nevertheless, this electron-hole-type symmetry is broken when J is odd except $J = 1$.

III. RESULTS AND DISCUSSIONS

We first consider the spin transport along the achiral nanotube with different sites contacted by the right lead, where the size of the nanotube is $J = 6$ and $N = 20$. Figure 2(a) presents the spin-up conductance $G_\uparrow$ and the spin-down one $G_\downarrow$ as a function of the Fermi energy E with $j = 1$, viz., the site {1,N} is connected to the right lead. One can identify several important features.

(i) A number of sharp peaks, associated with deep valleys, can be clearly seen in the transmission spectrum of $G_\uparrow$ and $G_\downarrow$. This oscillating behavior arises from the quantum interference effects, and both curves of $G_\uparrow$-E and $G_\downarrow$-E will be smoother by increasing the dephasing parameter Γ_d.

(ii) The spin-up and spin-down conductances satisfy $G_\uparrow(E) = G_\downarrow(-E)$, owing to the electron-hole-type symmetry mentioned above.

(iii) The curve of $G_\uparrow$-E is superimposable upon that of $G_\downarrow$-E, i.e., $G_\uparrow(E) = G_\downarrow(E)$ as expected, because the molecule is achiral and the mirror symmetry is preserved
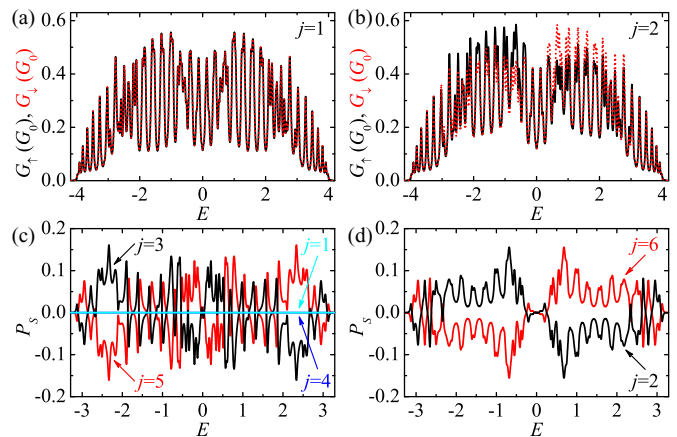
FIG. 2. Spin transport along the achiral molecule with site {1,1} always coupled to the left lead and site {j,N} connected to the right lead. Spin-up conductance $G_\uparrow$ (black solid line) and spin-down one $G_\downarrow$ (red dotted line) with (a) $j = 1$ and (b) $j = 2$, as a function of the Fermi energy E. (c), (d) Spin polarization P_s vs E with different sites {j,N} coupled to the right lead. Here, G_0 is the conductance quantum, the number of chains is $J = 6$, and the length is $N = 20$.

for the two-terminal setup. Consequently, the spin filtering phenomenon cannot be observed in the two-terminal achiral nanotube with $j = 1$ and the spin polarization is exactly zero, as evident by the cyan line in Fig. 2(c). This is independent of the model parameters.

(iv) Both curves of $G_\uparrow$-E and $G_\downarrow$-E are symmetric with respect to the line of $E = 0$, i.e., $G_\delta(E) = G_\delta(-E)$ with $\delta = \uparrow, \downarrow$. These equations are deduced from the coexistence of both the electron-hole-type symmetry and the mirror symmetry, and become invalid if one of the two symmetries is broken.

Figure 2(b) displays $G_\uparrow$ and $G_\downarrow$ as a function of E with $j = 2$. Although the aforementioned points (i) and (ii) are still maintained, a fundamental distinction can be observed from Fig. 2(b) that $G_\uparrow$ is different from $G_\downarrow$, which leads to the spin filtering phenomenon. This is unexpected for the achiral nanotube, because the helical symmetry, which is the key factor to yield the spin selectivity effect as indicated by a great deal of previous works [9,21–41], is absent in the achiral molecules. The underlying physics originates from the breaking of the mirror symmetry, which is caused by contact asymmetry between the left/right lead and the molecule. By inspecting Fig. 1, it is evident that when the site $\{2, N\}$ is coupled to the right lead, the two-terminal setup cannot be superimposed on its mirror image, although the nanotube itself is superimposable upon the mirror image. As a result, the mirror symmetry is broken for this two-terminal achiral molecule and gives rise to nonzero spin polarization P_s, as illustrated by the black line in Fig. 2(d).

Figures 2(c) and 2(d) show the spin polarization P_s versus E for the achiral nanotube with a single site $\{j, N\}$ contacted by the right lead, where j ranges from 1 to J. P_s is zero exactly for $j = 4$ as well, which is identical to the case of $j = 1$, since the mirror symmetry holds for both two-terminal setups. Nevertheless, when the other sites are connected to the right lead, the spin selectivity effect will emerge in the achiral molecule and some significant characteristics can be demonstrated.

(i) There exists a series of peaks and valleys in all the curves of P_s-E, which is irrespective of j, owing to the quantum interference effects.

(ii) Each curve of P_s-E is centrally symmetric for a specific j, i.e., $P_s(E) = -P_s(-E)$. This equality is expected from the general consideration of the electron-hole-type symmetry.

(iii) The spin polarization is considerably large, with the maximum value of P_s being 16% for $j = 3$ ($j = 5$) and 15% for $j = 2$ ($j = 6$). This implies that the achiral molecule can act as an efficient spin filter, which is comparable to the α-helical proteins [29,31].

(iv) By employing the reflection operation, the two-terminal setup with $j = 3$ is changed into the one with $j = 5$. In other words, the two-terminal setups with $j = 3$ and 5 are mirror images of each other. Then, the spin-up (spin-down) conductance of $j = 3$ is the same as the spin-down (spin-up) one of $j = 5$,[30] and the spin polarization is reversed exactly, i.e., $P_s(j = 3) = -P_s(j = 5)$ [Fig. 2(c)]. A similar phenomenon can also be observed for the system with $j = 2$ and 6 that $P_s(j = 2) = -P_s(j = 6)$ [Fig. 2(d)].

To demonstrate robustness of the spin selectivity effect of the achiral molecule, we then study its spin transport property
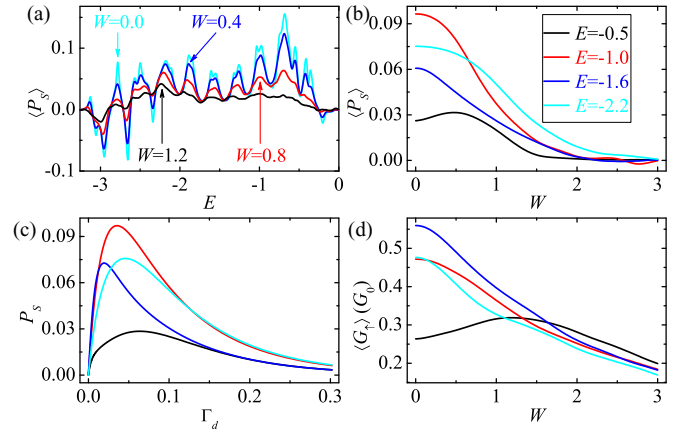
FIG. 3. Robustness of the spin selectivity effect of the achiral molecule against Anderson disorder and dephasing. (a) Averaged spin polarization $\langle P_s \rangle$ vs the Fermi energy E and (b) $\langle P_s \rangle$ vs disorder strength W, where the results are calculated from 10^3 disorder configurations. (c) P_s vs dephasing strength Γ_d and (d) averaged spin-up conductance $\langle G_\uparrow \rangle$ vs W. The different lines in panels (b), (c), and (d) represent typical values of E, and the other parameters are the same as Fig. 2(b).

by considering on-site energy disorder and various dephasing strengths. In the experiments, disorder and impurities exist inevitably, which will give rise to potential-energy differences. Here, the Anderson disorder is introduced into the diagonal term such that the nanotube potential energies distribute randomly within the range $[-W/2, W/2]$, with W the disorder strength. Figure 3(a) plots averaged spin polarization $\langle P_s \rangle$ versus E for different W, while Fig. 3(b) shows $\langle P_s \rangle$ versus W for typical values of E. Here, the averaged spin polarization is defined as $\langle P_s \rangle = (\langle G_\uparrow \rangle - \langle G_\downarrow \rangle)/(\langle G_\uparrow \rangle + \langle G_\downarrow \rangle)$, with averaged conductances $\langle G_\uparrow \rangle$ and $\langle G_\downarrow \rangle$ calculated from an ensemble of 10^3 disorder configurations. One can see from Fig. 3(a) that the oscillation amplitude of $\langle P_s \rangle$ is gradually declined by increasing W and the spin filtration efficiency is suppressed by the disorder, especially in the regions around the peaks. However, the spin selectivity effect is robust against the disorder. For instance, $\langle P_s \rangle$ can achieve 12% for $W = 0.4$ [see the blue line in Fig. 3(a)], which is about one order of magnitude larger than the SOC strength. Furthermore, $\langle P_s \rangle$ can be enhanced in the weak disorder regime [see the black line in Fig. 3(b)], especially for the Fermi energies around the valleys. Figure 3(d) presents $\langle G_\uparrow \rangle$ versus W. It clearly appears that $\langle G_\uparrow \rangle$ decreases with increasing W in general, which is expected from the disorder-induced Anderson localization in the nanoscaled systems. Nevertheless, in the regions around the valleys, $\langle G_\uparrow \rangle$ can be slightly increased by the weak disorder [see the black line in Fig. 3(d)], owing to the increment of density of states at this Fermi energy. In particular, $\langle G_\uparrow \rangle$ remains extremely large in the case of strong disorder and is approximately $0.2G_0$ for $W = 3$.

Figure 3(c) displays the spin polarization P_s versus the dephasing strength Γ_d. In fact, the dephasing possesses two roles [24,30]. On the one hand, the dephasing improves the openness of the molecule by coupling each site to a Büttiker virtual lead, which gives rise to the spin selectivity effect
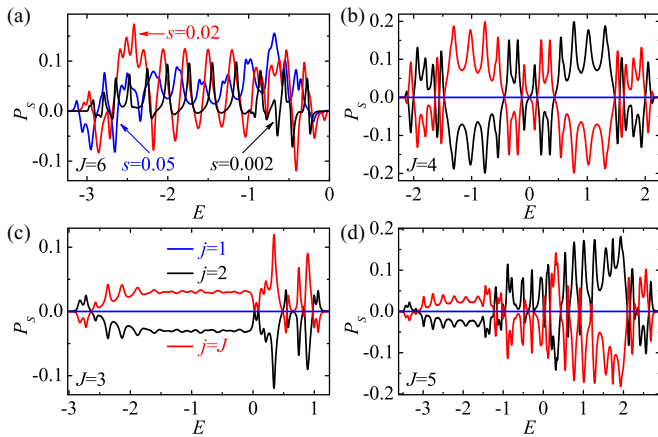
FIG. 4. Spin selectivity effect of the achiral molecule with various SOC strengths s and number of chains, J. (a) P_s vs E with three values of s for $J = 6$ and $j = 2$. (b)–(d) P_s vs E with $J = 4$, 3, and 5, where the different lines show that different sites $\{j, N\}$ are connected to the right lead. The other parameters are the same as Fig. 2(b).

[53]. This role of the dephasing is dominant when it is not quite strong and then P_s increases with Γ_d at first. On the other hand, the dephasing, which is introduced to simulate the inelastic-scattering events, leads to the loss of the electron phase memory and subsequently suppresses the spin selectivity effect. The second role of the dephasing competes with the first one and becomes dominant in the strong dephasing regime. In this situation, P_s is slowly declined by further increasing Γ_d. As a result, the dependence of P_s on Γ_d is not monotonic, which is independent of E. It is expected that the spin selectivity effect could also appear in the achiral molecule in the absence of the dephasing when it is contacted by multiple real leads [54].

Figure 4(a) displays P_s for the achiral nanotube with various SOC strengths s, as a function of E. It clearly appears that although the oscillating behavior is diverse for different s, the spin filtration efficiency remains significant even for very small SOC strength. P_s can reach 17% when $s = 0.02$ and 10% when $s = 0.002$, which is three orders of magnitude smaller than the hopping integral. From the above discussions, we conclude that the achiral molecule can be an efficient spin filter, because of considerably large P_s in the region of very weak SOC and the robustness against the disorder and the dephasing.

To explore the generality of the spin selectivity effect, Figs. 4(b)–4(d) show the spin polarization P_s versus E for

various achiral nanotubes with different number of chains, J. P_s is zero for all the achiral nanotubes with $j = 1$ as expected [see the blue lines in Figs. 4(b)–4(d)], due to the mirror symmetry. When the other sites are connected to the right lead, the spin selectivity effect appears [see the black and red lines in Figs. 4(b)–4(d)], regardless of the number of chains, since the mirror symmetry is broken for all these two-terminal setups. P_s is dramatically large for the achiral nanotubes with different radii, and achieves 12%, 20%, and 18% for $J = 3$, 4, and 5, respectively. When $J = 4$, $P_s(E) = -P_s(-E)$ always holds for a certain j [Fig. 4(b)], which is the same as $J = 6$, because the electron-hole-type symmetry is preserved for even J. When $J = 3$ and 5, $P_s(E) = -P_s(-E)$ becomes invalid [Figs. 4(c) and 4(d)], owing to the breaking of the electron-hole-type symmetry. P_s is reversed when the two-terminal setups are mirror images of each other, i.e., $P_s(j = 2) = -P_s(j = J)$, that is independent of the model parameters. Therefore, the spin selectivity effect may be a general phenomenon for the achiral molecules, and will appear by properly connecting to the leads so that the mirror symmetry is broken in the systems.

IV. CONCLUSIONS

In summary, a model Hamiltonian is proposed to study spin-dependent electron transmission through achiral nanotubes, which are contacted by two normal metal leads. The spin selectivity effect is demonstrated in the achiral nanotubes that by properly connecting to the leads, the injected unpolarized electrons are highly spin polarized after transmitting through the two-terminal setups, although the nanotubes themselves lack the chiral/helical symmetry. The spin selectivity effect is robust against disorder and dephasing. We envision that these findings could be detected in the experiments due to advanced nanotechnology. These results expand the spin selectivity effect to a wide range of the achiral molecules, and will help in engineering reliable molecule-based spin filters and memory devices.

[1] S. A. Wolf, D. D. Awschalom, R. A. Buhrman, J. M. Daughton, S. von Molnár, M. L. Roukes, A. Y. Chtchelkanova, and D. M. Treger, Science **294**, 1488 (2001).

[2] I. Žutić, J. Fabian, and S. Das Sarma, Rev. Mod. Phys. **76**, 323 (2004).

[3] D. D. Awschalom and M. E. Flatté, Nat. Phys. **3**, 153 (2007).

[4] A. Fert, Rev. Mod. Phys. **80**, 1517 (2008).

[5] J. Sinova, S. O. Valenzuela, J. Wunderlich, C. H. Back, and T. Jungwirth, Rev. Mod. Phys. **87**, 1213 (2015).

[6] L. Bogani and W. Wernsdorfer, Nat. Mater. **7**, 179 (2008).

[7] S. Sanvito, Chem. Soc. Rev. **40**, 3336 (2011).

[8] A. Saraiva-Souza, M. Smeu, L. Zhang, A. G. S. Filho, H. Guo, and M. A. Ratner, J. Am. Chem. Soc. **136**, 15065 (2014).

[9] R. Naaman and D. H. Waldeck, Annu. Rev. Phys. Chem. **66**, 263 (2015).

[10] Z. H. Xiong, D. Wu, Z. V. Vardeny, and J. Shi, Nature (London) **427**, 821 (2004).

[11] M. Urdampilleta, S. Klyatskaya, J.-P. Cleuziou, M. Ruben, and W. Wernsdorfer, Nat. Mater. **10**, 502 (2011).

[12] S. W. Jiang, S. Liu, P. Wang, Z. Z. Luan, X. D. Tao, H. F. Ding, and D. Wu, Phys. Rev. Lett. **115**, 086601 (2015).

[13] A. Smogunov and Y. J. Dappe, Nano Lett. **15**, 3552 (2015).

[14] D. Li, Y. J. Dappe, and A. Smogunov, Phys. Rev. B **93**, 201403(R) (2016).

[15] H. B. Heersche, Z. de Groot, J. A. Folk, H. S. J. van der Zant, C. Romeike, M. R. Wegewijs, L. Zobbi, D. Barreca, E. Tondello, and A. Cornia, Phys. Rev. Lett. **96**, 206801 (2006).

[16] M. Mannini, F. Pineider, C. Danieli, F. Totti, L. Sorace, Ph. Sainctavit, M.-A. Arrio, E. Otero, L. Joly, J. C. Cezar, A. Cornia, and R. Sessoli, Nature (London) **468**, 417 (2010).

[17] D. N. Woodruff, R. E. P. Winpenny, and R. A. Layfield, Chem. Rev. **113**, 5110 (2013).

[18] M.-H. Jo, J. E. Grose, K. Baheti, M. M. Deshmukh, J. J. Sokol, E. M. Rumberger, D. N. Hendrickson, J. R. Long, H. Park, and D. C. Ralph, Nano Lett. **6**, 2014 (2006).

[19] R. Vincent, S. Klyatskaya, M. Ruben, W. Wernsdorfer, and F. Balestro, Nature (London) **488**, 357 (2012).

[20] S. Thiele, R. Vincent, M. Holzmann, S. Klyatskaya, M. Ruben, F. Balestro, and W. Wernsdorfer, Phys. Rev. Lett. **111**, 037203 (2013).

[21] B. Göhler, V. Hamelbeck, T. Z. Markus, M. Kettner, G. F. Hanne, Z. Vager, R. Naaman, and H. Zacharias, Science **331**, 894 (2011).

[22] Z. Xie, T. Z. Markus, S. R. Cohen, Z. Vager, R. Gutierrez, and R. Naaman, Nano Lett. **11**, 4652 (2011).

[23] R. Naaman and D. H. Waldeck, J. Phys. Chem. Lett. **3**, 2178 (2012).

[24] A.-M. Guo and Q.-F. Sun, Phys. Rev. Lett. **108**, 218102 (2012).

[25] A.-M. Guo and Q.-F. Sun, Phys. Rev. B **86**, 035424 (2012).

[26] A.-M. Guo and Q.-F. Sun, Phys. Rev. B **86**, 115441 (2012).

[27] A. A. Eremko and V. M. Loktev, Phys. Rev. B **88**, 165409 (2013).

[28] R. A. Rosenberg, J. M. Symonds, V. Kalyanaraman, T. Markus, T. M. Orlando, R. Naaman, E. A. Medina, F. A. López, and V. Mujica, J. Phys. Chem. C **117**, 22307 (2013).

[29] D. Mishra, T. Z. Markus, R. Naaman, M. Kettner, B. Göhler, H. Zacharias, N. Friedman, M. Sheves, and C. Fontanesi, Proc. Natl. Acad. Sci. USA **110**, 14872 (2013).

[30] A.-M. Guo and Q.-F. Sun, Proc. Natl. Acad. Sci. USA **111**, 11658 (2014).

[31] M. Kettner, B. Göhler, H. Zacharias, D. Mishra, V. Kiran, R. Naaman, C. Fontanesi, D. H. Waldeck, S. Sęk, J. Pawłowski, and J. Juhaniewicz, J. Phys. Chem. C **119**, 14542 (2015).

[32] H. Einati, D. Mishra, N. Friedman, M. Sheves, and R. Naaman, Nano Lett. **15**, 1052 (2015).

[33] G. S. Diniz, A. Latgé, and S. E. Ulloa, Phys. Rev. Lett. **108**, 126601 (2012).

[34] K. M. Alam and S. Pramanik, Adv. Funct. Mater. **25**, 3210 (2015).

[35] V. Kiran, S. P. Mathew, S. R. Cohen, I. H. Delgado, J. Lacour, and R. Naaman, Adv. Mater. **28**, 1957 (2016).

[36] S. Yeganeh, M. A. Ratner, E. Medina, and V. Mujica, J. Chem. Phys. **131**, 014707 (2009).

[37] E. Medina, F. López, M. A. Ratner, and V. Mujica, Europhys. Lett. **99**, 17006 (2012).

[38] R. Gutierrez, E. Díaz, C. Gaul, T. Brumme, F. Domínguez-Adame, and G. Cuniberti, J. Phys. Chem. C **117**, 22276 (2013).

[39] J. Gersten, K. Kaasbjerg, and A. Nitzan, J. Chem. Phys. **139**, 114111 (2013).

[40] E. Medina, L. A. González-Arraga, D. Finkelstein-Shapiro, B. Berche, and V. Mujica, J. Chem. Phys. **142**, 194308 (2015).

[41] P. C. Mondal, N. Kantor-Uriel, S. P. Mathew, F. Tassinari, C. Fontanesi, and R. Naaman, Adv. Mater. **27**, 1924 (2015).

[42] *Organic Chemistry*, edited by J. Clayden, N. Greeves, and S. Warren (Oxford University, Oxford, England, 2012).

[43] J.-C. Charlier, X. Blase, and S. Roche, Rev. Mod. Phys. **79**, 677 (2007).

[44] M. J. Lagos, F. Sato, J. Bettini, V. Rodrigues, D. S. Galvão, and D. Ugarte, Nat. Nanotechnol. **4**, 149 (2009).

[45] P. A. S. Autreto, S. B. Legoas, M. Z. S. Flores, and D. S. Galvao, J. Chem. Phys. **133**, 124513 (2010).

[46] P. A. S. Autreto, M. J. Lagos, F. Sato, J. Bettini, A. R. Rocha, V. Rodrigues, D. Ugarte, and D. S. Galvao, Phys. Rev. Lett. **106**, 065501 (2011).

[47] S. Salehfar and S. Noorizadeh, Comput. Theor. Chem. **1027**, 1 (2014).

[48] P. Neuhaus, A. Cnossen, J. Q. Gong, L. M. Herz, and H. L. Anderson, Angew. Chem. Int. Ed. **54**, 7344 (2015).

[49] L. Miao, Q. Fan, L. Zhao, Q. Qiao, X. Zhang, C. Hou, J. Xu, Q. Luo, and J. Liu, Chem. Commun. **52**, 4092 (2016).

[50] N. J. Tao, Nat. Nanotech. **1**, 173 (2006).

[51] Y. Xing, Q.-F. Sun, and J. Wang, Phys. Rev. B **77**, 115346 (2008).

[52] *Electronic Transport in Mesoscopic Systems*, edited by S. Datta (Cambridge University, Cambridge, England, 1995).

[53] Q.-F. Sun and X. C. Xie, Phys. Rev. B **71**, 155321 (2005).

[54] A.-M. Guo, E. Díaz, C. Gaul, R. Gutierrez, F. Domínguez-Adame, G. Cuniberti, and Q.-F. Sun, Phys. Rev. B **89**, 205434 (2014).